The effect of temporal resolution of PAH emission data on transport and deposition patterns simulated with the Community Multiscale Air Quality modelling system (CMAQ)

I. Bewersdorff*, A. Aulinger, V. Matthias, M. Quante
GKSS Research Centre Geesthacht, Germany

Keywords: polycyclic aromatic hydrocarbon, PAH, air quality modelling, deposition, time-variant emissions

ABSTRACT: The effect of temporal variation of polycyclic aromatic hydrocarbon (PAH) emission data on transport and deposition patterns were simulated with the Community Multiscale Air Quality modelling system (CMAQ) for Europe, 54 km grid, for the year 2000. The carcinogenic benzo(a)pyrene (B(a)P) was used as a representative for the group of PAHs. The official emission data are only provided as one-year bulk emissions but the major emission sources of B(a)P vary within seasonal, diurnal and weekly cycles, respectively. The seasonal variability showed the greatest effects. However, on a regional scale diurnal cycles possessed significant effects as well. Comparison with measured weekly average concentration indicated the same trend for simulation and observation.

6 INTRODUCTION

Polycyclic aromatic hydrocarbons (PAHs) are semivolatile, lipophilic persistent organic pollutants (POPs), which originate primarily from incomplete combustion of organic material. Surveys have revealed that a variety of PAHs possess a high carcinogenic potential to animals and humans (ATSDR, 1995) and are bio-accumulated in the food chain. They can be transported over long distances in the atmosphere resulting in a widespread distribution across the earth, including regions where they have never been used. Due to their toxic and ecotoxic characteristics they pose a threat to humans and the environment, and therefore the international community has called for actions to reduce and eliminate the release of POPs, such as the Protocol to the UN-ECE Convention on Long-range Transboundary Air Pollution (CLRTAP) on POPs. Benzo(a)pyrene (B(a)P) is one of the best investigated PAHs both because of its severe toxicity and its relatively good availability to measurements. In our modelling study it was for this reason used as a marker for carcinogenic PAHs. The release of PAHs into the environment is highly dependent on human activities whereas their distribution over e.g. Europe is driven by their physical-chemical characteristics and meteorological conditions. Thus, to investigate the pathways of PAHs and to assess the threat they may pose to particular ecosystems it is indispensable to apply proper emission scenarios and meteorological data together with a sophisticated chemical transport model.

Significant emission sources of PAHs are residential combustion and road traffic both of which show considerable temporal variations. Residential combustion is mostly dependent on the season whereas traffic varies primarily within diurnal and weekly cycles. Since the meteorological conditions which drive the atmospheric transport model change with time the input emissions of the modelled compounds should present an appropriate temporal variation as well. It will make a significant difference in transport and deposition of pollutants whether high wind speeds, certain wind directions or precipitation events meet with emission peaks or time-invariant emissions. Emission data for B(a)P was provided to us by TNO (Denier van der Gon et al., 2005), but only as annual bulk emissions. In our study we present a first approach of implementing time-resolved B(a)P emissions. We then compared the model output of our B(a)P version of CMAQ when applying time- in-

* *Corresponding author:* Ines Bewersdorff, GKSS Research Centre Geesthacht, D-21502 Geesthacht, Germany. Email: ines.bewersdorff@gkss.de

variant emissions, emissions with only seasonal and weekly variability or with seasonal, weekly and diurnal variability. For validation purposes, the model results were also compared to B(a)P measurements in ambient air.
To evaluate the mean air concentrations the focus was put on the lowest model layer that is 35 m thick. Additionally, accumulated wet deposition patterns were investigated. Model runs were conducted for the months January, April, July and October that were selected as representatives for the whole year.

7 MODEL DESCRIPTION AND –SET UP

For the simulation of transport and chemical transformations the Models-3 Community Multiscale Air Quality (CMAQ) Modeling System was used (Byun and Ching, 1999; Byun and Schere, 2006). The CMAQ system consists of three primary components which are devoted to meteorology, emissions, and chemical transport, respectively. The chemistry transport module is mainly designed for classical air pollutants like SO_2, NO_x, O_3, and particulate matter (PM).

At GKSS the CMAQ systems was extended to cope with the transport of B(a)P in the gas phase and three particulate modes (Aulinger et al., 2006). Thereby, special emphasis was laid on considering the mass transfer of B(a)P between the gaseous and the particulate phase. Because the majority of our target substances is transported in the particulate phase the extended aerosol module of CMAQ (Binkowski and Roselle, 2003) is of primary importance for realistic simulations.

The meteorological fields were derived from MM5, the Fifth-Generation Pennsylvania State University/National Center for Atmospheric Research (NCAR) Mesoscale Model (Grell et al., 1995). Since wet deposition is the dominant sink for our applications, a more complex ice physics (Reisner 2 scheme) was employed and the Kain-Fritsch 2 convection scheme was used. The meteorological output fields were then processed using version 3 of Meteorology–Chemistry Interface Program (MCIP) for generating the input for the chemistry transport module.

MM5 as well as the CMAQ models were set up on a 54 x 54 km² grid for Europe, covering the entire North Sea and Baltic Sea in the North-West as well as the Mediterranean Sea and Black Sea in the South East. Thirty unevenly distributed vertical layers were used for all models employing a higher resolution in the atmospheric boundary layer. The meteorological model was run in a hindcast mode with six-hourly ERA-40 data (Uppala et al., 2005) as controlling input.

The chemistry model simulations used the CB-IV gas-phase chemistry mechanism and the efficient Euler Backward Interactive (EBI) solver. Fixed profiles of the relevant species were provided as boundary conditions. The model runs considered a spin-up of two days.

8 EMISSIONS

B(a)P emission data are available on the 50 x 50 km^2 polar stereographic EMEP grid as annual bulk emissions (Denier van der Gon et al., 2005) for eight emission sectors: Public power and heat, residential combustion, industrial combustion and processes, solvent and product use, road transport, non-road transport, waste incineration, agriculture. The major source, residential combustion, has a strong variability with the season and a lesser weekly and diurnal variability. The second important emission sector, industrial combustion and processes, is seasonally invariable and varies only within weekly and di-

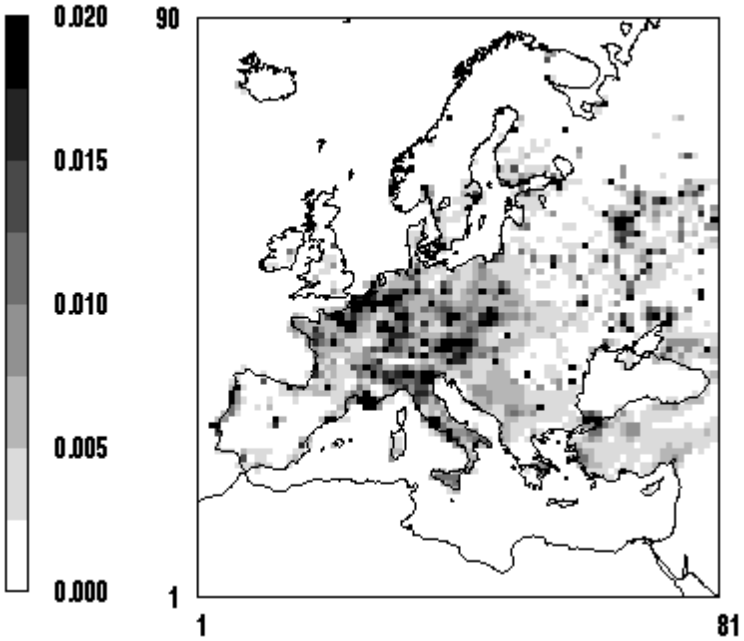

Figure 2. Average B(a)P emissions in g/s for 2000

urnal cycles. The latter is also true for emissions from road transport while the remaining sectors are negligible for B(a)P and are kept constant for simplicity. CMAQ requires emissions with a one hour time step. Three different temporally resolved emission data (cases A, B and C) sets were used as input data for CMAQ (Tab. 1).

Table 4. Overview of the three different temporally resolved emission data sets

	Temporal variations considered		
Case	Annual cycle	Weekly cycle	Daily cycle
A (constant)	-	-	-
B (seasonal)	+	+	-
C (daily)	+	+	+

At first, constant emissions for each hour of the year were generated to feed into the Eulerian air quality model (case A). In a second approach we employed seasonal variations of the emissions including annual and weekly cycles. In addition to the seasonal variation the third dataset with daily resolved emissions included also a diurnal cycle. Table 2 provides information on the different temporally resolved emission cycles that were applied to the annual bulk emissions.

Table 5. Temporally emission resolution

Emission resolution	Description
Constant emissions	Constant emissions each hour of the year
Annual cycle	Influenced by residential heating, deduced from B(a)P measurements in Kosetice, Czech Republic, which reflects the seasonal cycle (Holoubek et al., 1992)
Weekly cycle	Ascribed to working days, influenced by residential heating, traffic and industry
Daily cycle	Dependent on working hours, scaling factor deduced from NO emission variations for emissions originating from road traffic and CO emission variations for residential combustion

9 RESULTS AND DISCUSSION

9.1 *Regional distributions depending on different emission cycles*

In the entire model domain, the time-variant emissions lead to much higher B(a)P concentrations and depositions in January than in the other tested months due to the implemented annual cycle of B(a)P emissions which is dominated by residential heating. In January B(a)P concentrations up to 2.5 ng/m³ were modelled whereas in July in large parts of Europe the concentrations simulated with daily resolved emissions (case C) did not exceed 0.06 ng/m³. The B(a)P concentration level reached in winter could already cause noticeable human health effects (Hellmeier and Huhmann, 2001). Thus, figures of the B(a)P concentration and deposition distribution over Europe are only displayed for January (Figs. 2, 4, 6, 8).

9.1.1 *Comparison of case A with case B*

Although the total amount of annual emissions was kept constant, the mean annual concentrations were different – depending on the region – when running the model with constant (case A) or seasonally/weekly resolved emissions (case B). Figure 3 shows that especially in the region north of the Black Sea, in parts of the European part of Russia and in the area from Slovenia over Austria and Slovakia to Poland estimated B(a)P concentrations were significantly higher when considering the seasonal cycle. Even larger differences could of course be observed in the monthly mean concentrations. In January the differences between cases A and B were more pronounced than in the other investigated months (Fig. 7).

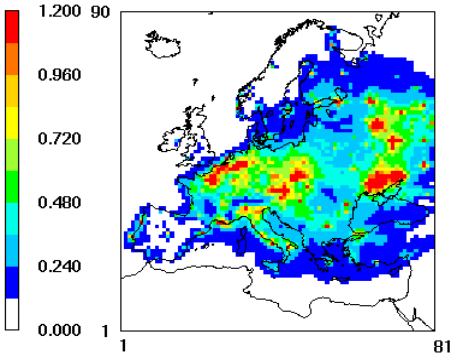

Figure 2: Average annual ground level concentrations in ng/m^3 (case A)

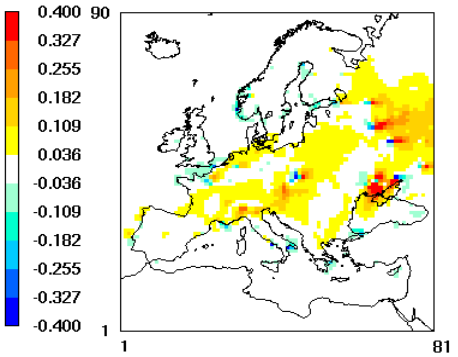

Figure 3: Differential plots of annual mean concentrations in ng/m^3; case B - case A

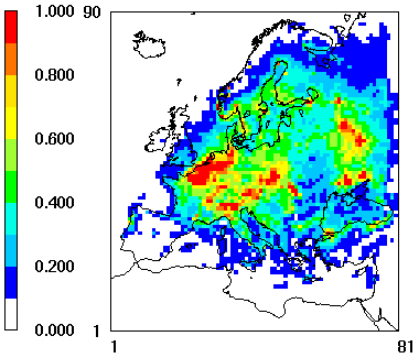

Figure 4: Annual depositions in g/hectare (case A)

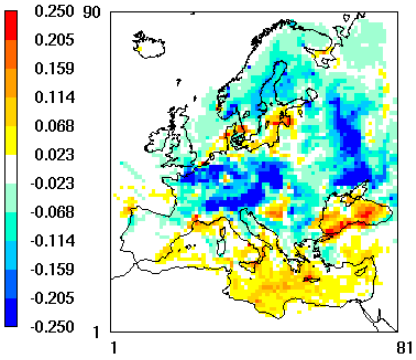

Figure 5: Differential plots of annual depositions in g/hectare; case B - case A

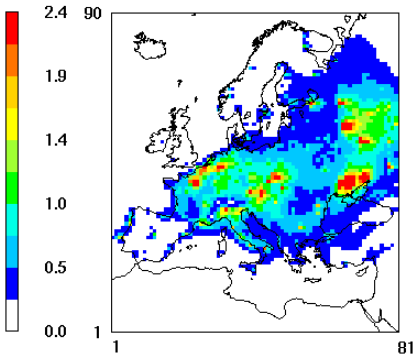

Figure 6: Average ground level concentrations in January in ng/m^3 (case A)

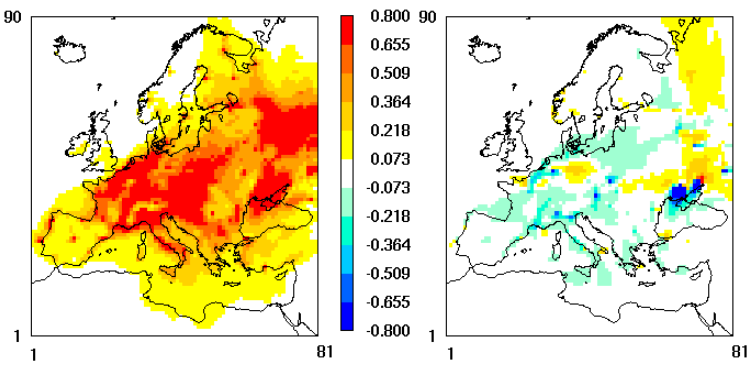

Figure 7: Differential plots of ground level concentrations in January in ng/m^3; left: case B - case A; right: case C - case B

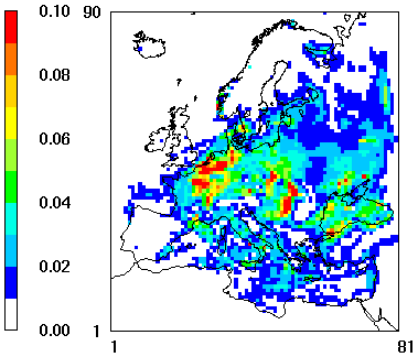

Figure 8: Depositions in January in g/hectare (case A)

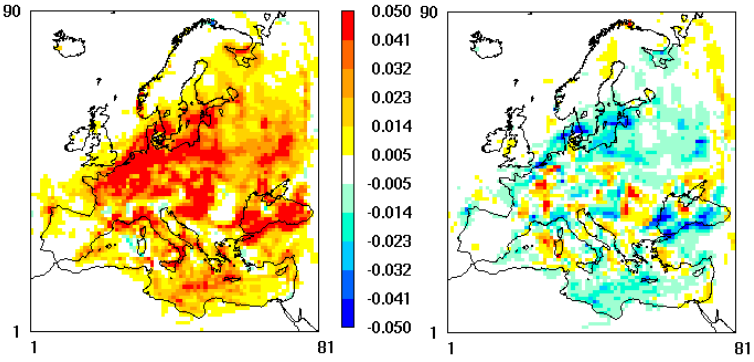

Figure 9: Differential plots of depositions in January in g/hectare; left: case B - case A; right: case C - case B

The concentrations showed an increase by at least 70 %, but reached up to 130 % over the North Sea and in the north of the Black Sea. In contrast, in April and July the B(a)P concentrations were decreased, in April by around 40 % and in July by around 90 % October showed no general trend. In some regions the differences were -10 % and in other regions +10 %. The differences in monthly depositions reflected in general the differences in concentrations (Figs. 5, 9). The application of time-variant emissions lead to increased B(a)P deposition in January, from 0.02-0.04 g/ha to 0.03-0.1 g/ha over a wide area of Europe, but especially in Central Europe and over the Black Sea. In July the depositions with constant emissions ranged from 0.03-0.07 g/ha. With seasonally resolved emissions they decreased by over 90 %. Furthermore, April showed a Europe-wide decrease of deposition with annual and weekly cycles as well, but with a more moderate slope. In April the depositions dropped off between 30 % and 50 %. The Differences in October amounted to -30 % up to +30 %.

9.1.2 *Comparison of case B with case C*

The differences of model results between simulations with the seasonal and daily cycle turned out lesser and at smaller regional scales (Fig. 7). In January again the differences were most pronounced. In the greater Moscow area the concentrations for case C were up to 50 % elevated compared to the results from emissions with seasonal variations (case B). Other spots of increased B(a)P concentrations for case C could be observed in the centre of Europe (Germany and Poland) where the concentrations rose by approximately 25 %. In July, where the concentration of B(a)P hardly exceeded 0.03 ng/m³, the differences between cases B and C were still visible but significantly smaller – at most 10 % – than in January. Concerning the annual mean concentrations between case B and C reveals that mainly in the area north of the Black Sea a decrease of the B(a)P concentration is noticed.

The differences of the depositions between the seasonal and diurnal cycle draw a comparable picture as described for the concentration deviations (Fig. 9). Between the two different time-variant emission cycles (case B and C) January are responsible for the main deviation to the annual B(a)P depositions which accounts for 50 % in some parts of Europe, e. g. parts of Poland, Romania and Bulgaria. During the other months in most areas of Europe the difference is not larger than +/-10 %.

9.2 *Comparison with ground measurements*

B(a)P ground level measurements from two sites belonging to the air quality assessment program of UBA (German Federal Environmental Agency) were used to evaluate the simulated concentrations in the lowest model layer. At Bornhoeved, a rural site in the north of Germany, the measurement data were provided as weekly average concentrations and at Radebeul, an urban site in the east of Germany, as daily average concentrations. Thus, weekly and daily averages were calculated from the model output that has a time resolution of one hour. Predominantly, all three approaches with differently time-variant emission files described the same trend as the measurements. For both tested sites the concentration levels calculated with cases B and C diverged only at the most 10 % from each other, whereas the differences between cases A and B were up to 75 % in January and 94 % in July. For Bornhoeved the simulations constantly overestimated the B(a)P concentrations. The largest deviation was found in January where the simulated monthly mean with case C was 400 % above the measured mean and 200 % with case A. In July, in contrast, the deviation was only 6 % with case C while 1500 % with case A. At Radebeul the simulated monthly mean concentration was 8 % (case C) higher or 40 % lower (case A) and in July 265 % higher with case A and 77 % lower with case C than the measured one. In general, the case C simulations fitted best to the observations.

Taking into account that it cannot be assured that the measurement sites are representative for the entire grid cell in which they lie and that the shape of the concentration curves is well reproduced by the simulations the performance of the model can be regarded as acceptable. Differences in absolute values between measurements and simulations may rather be owed to uncertainties in absolute emissions.

10 CONCLUSION

As expected, the results confirmed that seasonally resolved emission data has a Europe-wide effect on the simulated B(a)P concentrations and depositions. A diurnal cycle induces significant effects on a regional scale solely. The greatest influences of time-variant emissions were observed in January, in April and July the effects were less pronounced and the least in October. A comparison with ground level measurements showed that the simulations reflect the observed trends in concentration. However, the deviations depend strongly on the site, industrialised or rural area, and the month considered.

The seasonal variability of emissions as it was employed in this study reflects the seasonality only at one particulate site in the Czech Republic which is probably not representative for the whole model domain. In order to reflect a locally specific seasonality, we will proceed by creating emissions that are directly correlated with the temperature in each grid cell.

None the less it is evident that emissions that vary with the season are an indispensable prerequisite for realistic model results. We regard it even as recommendable to include a daily cycle as well to achieve a better spacial resolution of concentration and deposition patterns. A more representative evaluation of the model results could only be achieved with data of long-term studies which should include several seasonal cycles.

11 ACKNOWLEDEMENTS

TNO Netherlands is gratefully acknowledged for providing emission data of B(a)P. Furthermore, we thank IER Stuttgart for providing emission data of main pollutants and the German Federal Environment Agency is acknowledged for the use of measurement data.

REFERENCES

ATSDR (Agency for Toxic Substances and Disease Registry), 1995: *Toxicological Profile for Polycyclic Aromatic Hydrocarbons (PAHs)*. Public Health Service, US Department of Health and Human Services, Atlanta, GA, USA.

Aulinger, A., V. Matthias, and M. Quante, 2006: Introducing a partitioning mechanism for PAHs into the Community Multiscale Air Quality modelling system and its application to simulating the transport of benzo(a)pyrene over Europe. *submitted to J. Appl. Meteorol.*

Binkowski, F.S. and S.J. Roselle, 2003: Models-3 Community multiscale air quality (CMAQ) model aerosol component, 1 Model description. *J. Geophys. Res. 108(D6)*, 4183, doi:10.1029/2001JD001409.

Byun, D. and J.K.S. Ching, 1999: *Science Algorithms of the EPA Models-3 Community Multyscale Air Quality Modelling System*. EPA report, EPA/600/R-99/030, Office of Research and Development, Washington DC 20406.

Byun, D., and K.L. Schere, 2006: Review of the Governing Equations, Computational Algorithms, and Other Components of the Models-3 Community Multiscale Air Quality (CMAQ) Modeling System. *Appl. Mech. Rev. 59*, 51-77.

Denier van der Gon, H.A.C., M. van het Bolscher, A.J.H. Visschedijk, and P.Y.J. Zandveld, 2005: *Study of the effectiveness of UNECE Persistent Organic Pollutants Protocol and cost of possible additional measures. Phase I: Estimation of emission reduction resulting from the implementation of the POP Protocol*. TNO-report. B&O-A R 2005/194. Appeldoorn, Netherlands.

Grell, G.A., J. Dudhia, and D.R. Stauffer, 1995: *A Description of the Fifth-Generation Penn State/NCAR Mesoscale Model _MM5.* NCAR Technical Note, NCAR/TN-398+STR, Boulder, CO, 138 pp.

Hellmeier, W. and H. Huhmann, 2001: Gesundheitsindikator 5.8, Polycyclische, aromatische Kohlenwasserstoffe (PAK) in der Außenluft. Landesinstitut für den öffentlichen Gesundheitsdienst, http://www.loegd.nrw.de/1pdf_dokumente/4_umweltmedizin_umwelthygiene/kommentierung_indikatoren_umwelt/ind_5-8_ueberarbeitet_01_2001.pdf, 15.09.2006.

Holoubek, I. and 11 authors, 1992: Project TOCOEN - The Fate of Selected Organic Compounds in the Environment. Part XI. The PAHs, PCBs, PCDDs/Fs in Ambient Air at Area of Background GEMS Station. Seasonal Variations. *Toxicol. Environ. Chem*., 36, 115-123.

Uppala S.M. and 44 authors, 2005: The ERA-40 reanalysis. *Quart. J. Roy. Meteor. Soc. 131*, 2961-3012.

Physical Characterization of PM Emissions from In-Service Commercial Gas Turbine Engines – Projects APEX and JETS APEX2

D.E. Hagen*, P. Lobo, P.D. Whitefield
University of Missouri – Rolla Center of Excellence for Aerospace Particulate Emissions Reduction Research, Rolla, MO, USA

Keywords: APEX, JETS APEX2, PM emissions, CFM56

ABSTRACT: On-wing PM measurements were made on GE CFM56 class engines at the exhaust nozzle exit (~1m) and at downstream locations (30m and 50m) in the near field plume. At the engine exit plane, size distributions were generally lognormal. EIn – number-based emission index was a minimum at mid-level thrusts compared to the idle and high thrust settings. For measurements made at downstream locations in the near-field plume, the onset of gas-to-particle conversion was apparent for low to medium thrusts. Non-lognormal size distributions were often observed where the mean sizes (~12-15nm) were found to be smaller than the 1m case. EIn also decreased with increasing thrust, and was an order of magnitude higher than that for the engine exit cases at low thrusts. EIm – mass-based emission index was found to increase with thrust, ranging from 0.001-0.37 g/kg fuel burnt.

1 INTRODUCTION

The University of Missouri – Rolla (UMR) Center of Excellence was involved in two recent ground-based aircraft emissions measurement campaigns – Project APEX (NASA Dryden Flight Research Center, April 2004) and JETS APEX2 (Oakland International Airport, August 2005). The goal of these studies was to advance the understanding of particle emissions and their evolution in the atmosphere from in-service commercial gas turbine engines. Extractive particulate matter (PM) emission measurements were made on GE CFM56 class engines at the exhaust nozzle exit (~1m) and at downstream locations (30m and 50m) in the near field plume. The roles of fuel composition and engine power setting were also explored. These engines were mounted on three airframes: DC8-50, B737-300, and B737-700. These measurement campaigns involved a multi-agency team: NASA (DFRC, GRC, LaRC), EPA, FAA, DoD (AEDC, NAVAIR, NFESC, WPAFB), Aviation Industry (GE, Boeing, PW), and Research Community (ARI, MIT, PM, UCF, UCR, UMR).

At Project APEX, three different fuels were used – a baseline JP-8 fuel (Base Fuel - 383 ppmm sulfur and 17.6% aromatics), Base Fuel doped with tertiary butyl disulfide (High Sulfur Fuel - 1595 ppmm sulfur and 17.3% aromatics), and Jet A fuel which had a considerably higher aromatic content than the two other fuels used (High Aromatic Fuel - 530 ppmm sulfur and 21.6% aromatics). Fuel sulfur and aromatic concentrations reported are in parts per million mass and % by volume, respectively. The fuel for JETS APEX2 was JET A having a total aromatics in the range 19.6-22.8% by volume and a sulphur content ranging from 125-419 ppmm. At both these tests, the test matrix consisted of a modified LTO cycle with power settings of 4%, 5.5%, 7%, 15%, 30%, 40%, 60%, 65%, 70%, 85% and 100%. The times on each power condition were nominally 4 minutes, except for the 100% case which was limited to 1.5 minutes. At Project APEX, the test aircraft was parked on a pad. In contrast at JETS APEX 2, the aircraft was parked at a Ground Runup Enclosure which eliminated problems associated with changing wind directions.

* *Corresponding author:* Donald E. Hagen, UMR Center of Excellence for Aerospace Particulate Emissions Reduction Research, G-7 Norwood Hall, University of Missouri – Rolla, Rolla, MO 65409, USA. Email: hagen@umr.edu

2 SAMPLING TRAIN AND INSTRUMENTATION

Custom-designed probes and extensive support equipment were used to sample jet exhaust in the on-wing position. Particle-laden exhaust was extracted directly from the engine exhaust flow through probes and supplied to the measurement devices. The primary probe for collecting samples and data was positioned within 1 meter of the exhaust nozzle exit plane, as this position is representative of the engine signature and the certification data in the International Civil Aviation Organization (ICAO) database (ICAO, 2006). The PM probes are designed to provide both probe tip and upstream (0.09 meters from tip) dilution flows, thereby reducing and/or eliminating probe effects. The rake quadrant and probes are water cooled to protect them from thermal degradation during testing. The dilution flows are drawn from particle-free, dry air sources located in the mobile laboratories and conducted to the probes through 0.006-meter (inside diameter) flexible gas lines. The sample for PM measurements are conducted to the mobile laboratories through a ¾" SS sample line for which line losses have been calibrated.

Dry nitrogen for dilution was introduced into the flow at the probe tips on the 1m rakes. The dilution was used to suppress particle-particle interactions and gas-to-particle conversion. The amount of dilution gas was controlled by observing the CO_2 concentration in the sample line and keeping it at a desired level. Typical dilution ratios were in the range 10-40. No diluent was provided at the downstream locations since sufficient dilution with ambient air was found to have occurred naturally in the plume.

UMR has developed a state-of-the-art mobile diagnostic facility and a sophisticated sampling methodology for nanometre scale PM optimized for jet engine exhaust characterization (Schmid et al., 2004; Lobo et al. 2006). The instrumentation consists of 2 state-of-the-art fast particulate spectrometers (Cambustion DMS500) to gather real–time size distribution information and total concentration of engine exhaust PM; a differential mobility analyzer (DMA) (TSI model 3071), a more traditional tool for particle size measurement, sacrificing speed for greater sensitivity when compared to the DMS500; Condensation Particle Counters (CPCs) (TSI models 3022 and 3025) to measure total number concentration; a fast response carbon dioxide (CO_2) detector (Sable Systems model CA-2A) to monitor sample dilution and establish emission factors; and a weather station to monitor the ambient conditions of temperature, relative humidity, pressure, and wind speed and direction. Two fast particulate spectrometers were used to get both volatile and non-volatile particulate information. To achieve this differentiation, one of the spectrometers was preceded by a thermal denuder operating at 300^{o}C to remove volatile material.

3 RESULTS

Detailed data from Project APEX can be found at public website: http://particles.grc.nasa.gov and in the recently released NASA final report (Wey et al., 2006). Similar data for Project JETS APEX2 is anticipated to be released to the public in December 2006. In this paper the data for the CFM56 class of engines from both projects will be used to explore PM emissions dependencies on selected operational parameters.

Figure 1 shows the emission indices (EIn – number-based emission index, and EIm – mass-based emission index) as functions of power, fuel type, and distance downstream of the engine exit. There is a difference in EIn between the 1m and 30 m probe locations. At the 30m probe location, EIn is highest at the lowest power, and is an order of magnitude higher than that for the 1 case. It then decreases with power until ~85% is reached, where it becomes constant. The greatest differences between the 1m and 30m data are observed at low powers where the residence time in the plume affords more opportunity for gas-to-particle conversion to occur resulting in larger EIn values. For all three fuels, at both probe locations, EIm tends to increase with power, with a low power minimum near 20%, and a high power maximum above 85%. At high fuel flow rates, the EIm values for the 1 and 30m cases converge suggesting that the mass at these higher fuel flow rates is dominated by the non-volatile component of the aerosol.

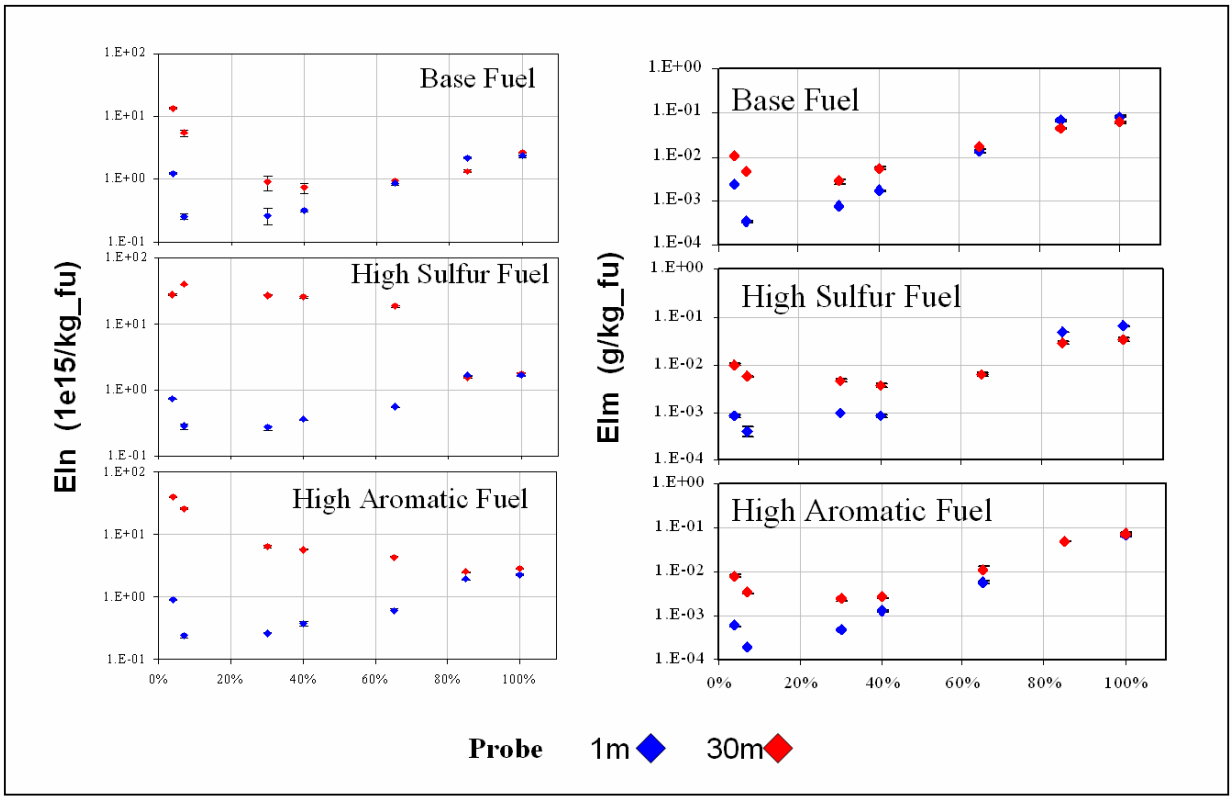

Figure 3. Emission indices as functions of power, fuel type and distance downstream of the engine exit

Figure 2 shows the engine to engine variability in emission indices (EIn and EIm) close to the engine exit plane (~1m) plotted versus power. All engines demonstrate the power dependence discussed above. However, engine to engine variance exceeded that associated with power change for a given engine. In the case of EIn, the new technology engines on the -700 series aircraft produce fewer particles per kilogram of fuel burned. This difference is large and statistically significant. Averaged across all powers, this difference represents a (79 ± 12) % reduction in number-based emissions normalized to fuel flow. EIn for the Project APEX engine falls between those of the -300 and -700 series and the differences between all engines are statistically significant at higher powers. Mass-based emission index exhibited a trend to increase with power. The trend is stronger for the older engine technology (-300 series). There is a large and statistically significant difference at high power representing a 72% reduction in mass-based emissions normalized for fuel flow at 85% power. This is also the case for the CFM56-2C1 engine studied in Project APEX.

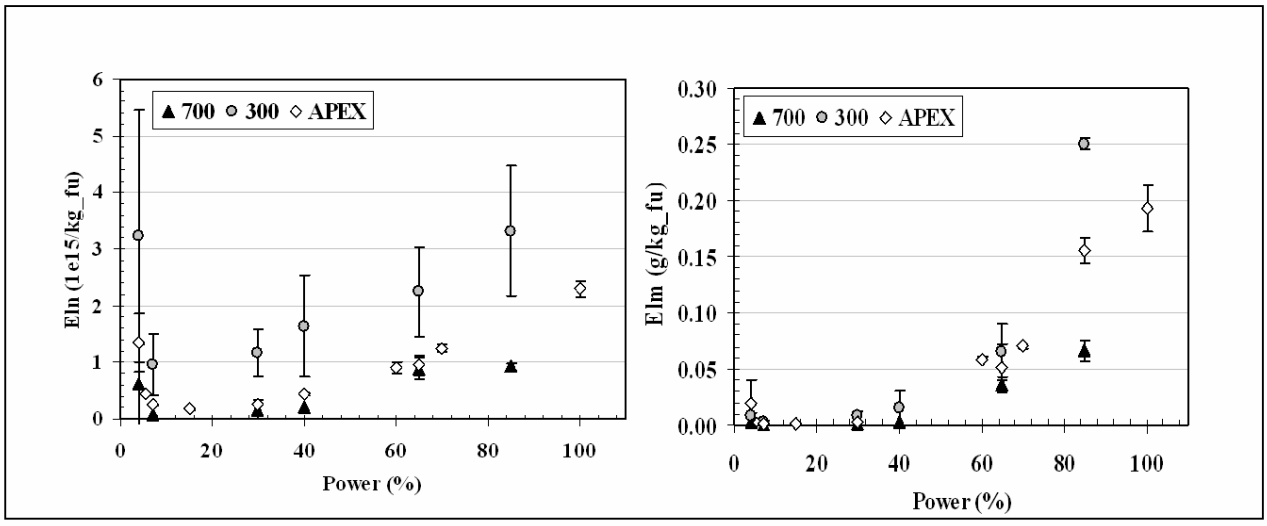

Figure 4. Engine to engine variability in emission indices

Figure 3 compares the emission indices (EIn and EIm) for the total aerosol and non-volatile component at the 50m sampling location. Plume processing in the expanding exhaust plume results in the production of a large number of small particles (volatile material) observed in the total aerosol but not present in the non-volatile component. The production of these small particles results in an order of magnitude increase in EIn. These particles also contribute to the mass dependent parameter values, but to a lesser extent.

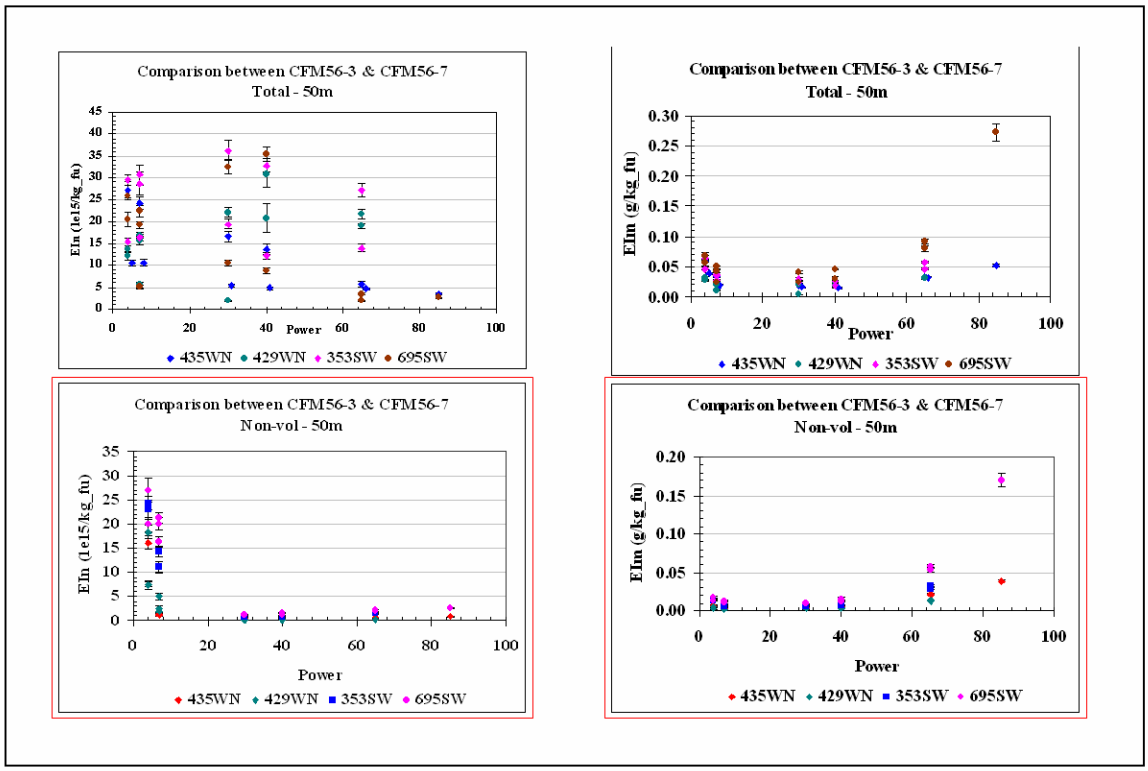

Figure 5. Comparison of emission indices for the total aerosol and non-volatile component at the 50m sampling location

Table 1 summarizes the range of PM parameter values measured for the CFM56 class of engines in these sampling campaigns, and compares them to published values for individual engine measurements using estimated size distributions.

Table 6. Range of PM parameter values measured for the CFM56 class of engines

Parameter	Min	±%	Max	±%	Average	±%	Slope
EIn (10^15/kg_fuel)							
Non-vol 1m	0.67	64	4.1	61	1.7	56	-
Non-vol plume	0.54	68	17.9	32	6.0	49	-
Total 1m	0.68	87	10.2	130	4.5	129	±
Total plume	7.95	85	28.0	38	16.1	28	-
IPCC (Penner et al. 1999)	0.30		50.0				
EIm (g/kg_fuel)							
Non-vol 1m	0.002	69	0.060	55	0.016	49	+
Non-vol plume	0.004	74	0.045	75	0.014	62	+
Total 1m	0.002	84	0.084	55	0.023	61	+
Total plume	0.012	65	0.078	52	0.031	47	±
IPCC (Penner et al. 1999)	0.010		0.200				

4 CONCLUSIONS

The following conclusions for the CFM56 PM Emission Indices can be drawn from the APEX and JETS APEX2 data sets when averaged for all powers and engines studied.

- Number-based emission indices exhibit a minimum at low to mid power, range from 0.5 to $28x10^{15}$/kg_fuel, and increase by as much as an order of magnitude with plume processing.
- Mass-based emission indices tend to increase with power and range from 0.002 to 0.08 g/kg_fuel, bound the fleet average estimated for the mid 1990s fleet (Döpelheuer, 1997), and are at the low end of emission index range reported for individual engines using estimated size distributions (Penner et al., 1999).
- Engine to engine variability is difficult to estimate when the engine sample size is small. The value of accurately estimating these parameters warrants further study. The experimental approach developed through the APEX series of studies provides the blueprint for future studies.

ACKNOWLEGEMENTS

The authors would like to acknowledge the sponsorship of California Air Resources Board, National Aeronautics and Space Administration, Federal Aviation Administration and the UMR Center of Excellence for Aerospace Particulate Emission Reduction Research throughout the work described in this paper.

REFERENCES

Döpelheuer,A. (1997). "Berechnung der Produkte unvollständiger Verbrennung aus Luftfahrttriebwerken. IB-325-09-97, Deutsche Zentrum für Luft- und Raumfahrt, Cologne, Germany, 38 pp.

ICAO, International Civil Aviation Organization *Aircraft Engine Emissions DataBank*. (2006)

Lobo, P., Hagen, D.E., and Whitefield, P.D. (2006). Physical characterization of aerosol emissions from a Commercial Gas Turbine Engine – Project APEX. submitted to the Journal of Propulsion and Power.

Penner, J. E., Lister, D. H., Griggs, D. J., Dokken, D. J., and McFarland, M. (eds.), *Aviation and the Global Atmosphere*, IPCC Report, Cambridge University Press, Cambridge, UK, 1999, p. 373

Schmid, O., Hagen, D., Whitefield, P., Trueblood, M., Rutter, A., and Lilenfeld, H. (2004). "Methodology for particle characterization in the exhaust flow of gas turbine engines", *Aerosol Sci. & Technol.* 38:1108-1122.

Wey, C.C., Anderson, B.E., Hudgins, C., Wey, C., Li-Jones, X., Winstead, E., Thornhill, L.K., Lobo, P., Hagen, D., Whitefield, P., Yelvington, P. E., Herndon, S.C., Onasch, T.B., Miake-Lye, R.C., Wormhoudt, J., Knighton, W.B., Howard, R., Bryant, D., Corporan, E., Moses, C., Holve, D., and Dodds, W. (2006) "Aircraft Particle Emissions eXperiment (APEX)" NASA TM-2006-214382

Aircraft Emissions Characterization

S.C. Herndon, T.B. Onasch, J.T. Jayne, E.C. Wood, P.E. Yelvington*, J. Wormhoudt, M.J. Northway, P. Mortimer, D.R. Worsnop, M.S. Zahniser, D.D. Nelson, J.H. Shorter, J.B. McManus and R.C. Miake-Lye
Aerodyne Research, Inc., MA 01821 USA

W. Berk Knighton
Department of Chemistry, Montana State University, USA

L.C. Marr
Virginia Tech, Blackburg, VA USA

B.E. Anderson, C.-L. Wey
NASA, Langley and Glenn Research Centers (respectively) USA

P.D. Whitefield
University of Missouri, Rolla,

Keywords: Aircraft engine, NO_x, CO, formaldehyde, particles, gaseous, hydrocarbon, emissions

ABSTRACT: Recent engine exhaust measurements have been performed to better characterize the gaseous and particle emissions from aircraft engines as a function of engine power and distance downstream in the exhaust plume. Speciation of NO_x and hydrocarbon emissions, and their dependence on engine power, have been quantified for engines that are used extensively in the commercial fleet. In addition to these gaseous species, non-volatile and volatile contributions to aerosol emissions have also been quantified, identifying sulfate and organic contributions to the volatile condensed mass at downstream plume locations. Sulfate mass emission indices (g/kg fuel), due to sulfur contained in the fuel, do not have a strong dependence on engine power, while organic mass emission indices are highest at low powers. Non-volatile particle mass emission indices increase strongly from low to high powers.

1 INTRODUCTION

The quantification of the emissions from an aircraft gas turbine engine is complicated by the high temperature and high velocity of the exhaust as it leaves the engine. In addition, many species of interest are present in low concentrations and detailed information is sought about the small particles emitted. Several recent studies (Whitefield et al., 2002; Anderson et al., 2005; Herndon et al., 2004, 2005, 2006, C.C. Wey et al., 2006, ARB, 2006) have been directed at tackling these challenging measurement problems in order to have better understanding of the emissions from aircraft engines and how they evolve immediately downstream of the engine so that better assessments of the environmental impacts can be performed.

A poster was prepared for the TAC meeting, which presented a wide range of measurement results from aircraft emissions measurements, spanning the range from

- At the exit of a combustor - as used in an aircraft engine but measured in a test rig that simulates the engine conditions,
- In the plume of an aircraft engine – with the engine mounted in a test facility or on a stationary aircraft, and sampled at the engine exit or various downstream locations (see Figure 1)
- From advected downwind plume – beside active runways, using fast time response instruments on a non-interference basis at commercial airports.

* *Corresponding author:* Paul Yelvington, Aerodyne Research Inc., 45 Manning Road, Billerica, Massachusetts, USA. Email: paul@aerodyne.com. This material does not necessarily represent the views or recommendations of the U.S. DOT and its agencies.

The data presented included both gaseous emissions data and measurements of particle emission parameters, focusing on data obtained in those studies by Aerodyne Research, Inc. Gas phase emissions measurements of NO, NO2, HONO, CO, and a variety of hydrocarbons were obtained using chemiluminescence, Tunable Infrared Laser Differential Absorption Spectroscopy (TILDAS), and Proton Transfer Reaction Mass Spectroscopy (PTR-MS). Particle measurements that were presented focused on those measured using Multi-Angle Absorption Photometry (MAAP), and Aerosol Mass Spectroscopy (AMS).

Figure 1. The APEX experiment measured emissions from a CFM56-2C1 engine mounted on the NASA DC-8 airplane. Measurements were performed using specially prepared sample probes and mounding rakes at 1, 10, and 30 m nominal distances downstream of the engine.

The breadth of data presented in the TAC poster is too extensive to include in this brief conference proceedings, but much of that data is available in the referenced papers and reports. An example of the particulate emissions data from APEX is presented in Figure 2, in which particle composition data is presented as a function of engine operating power. The mass associated with the emitted black carbon (soot) is the most notable feature (in black), which increased dramatically at high engine powers. The volatile contributions from sulfate (sulfuric acid) and organics vary much less with power, although the both increase when fuel sulfur content is increased (right panel). Notably, at low powers when the black carbon contribution decreases, the volatile components of the emitted particles become more significant. These volatile contributions are compared in the figure with masses inferred from particle size distributions measured with an SMPS, but note that the SMPS measures particles to a smaller size than the AMS (sulfate and organic). Thus the volatile volume from the SMPS (lines with symbols) is greater than the sum of sulfate and organic from the AMS, due to many small volatile particles less than the AMS ~30 nm cutoff.

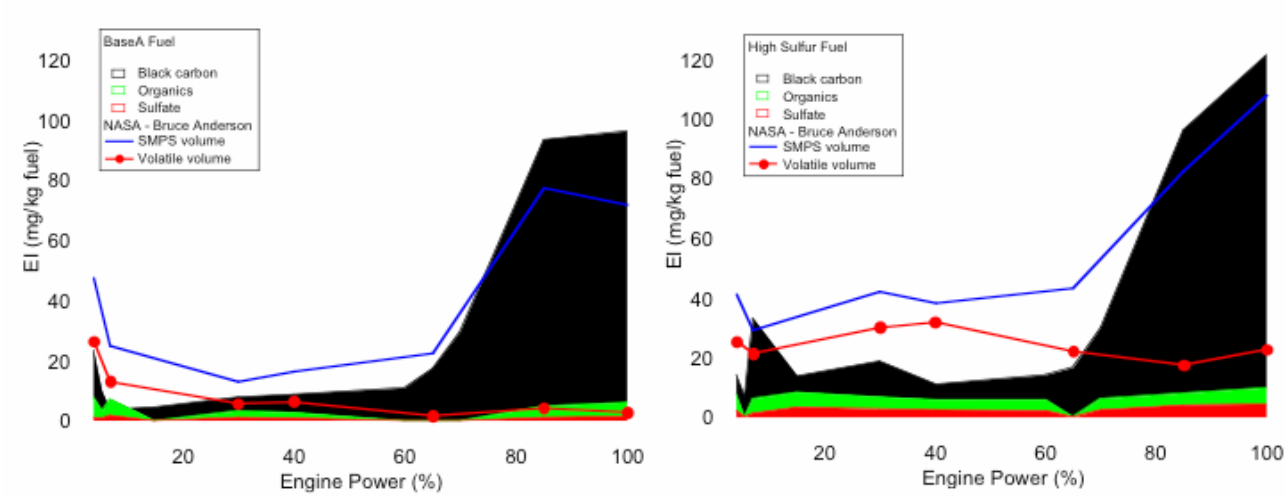

Figure 2. The composition of emitted particles is plotted versus engine power for the APEX engine measurements. The shaded-in contributions represent black carbon (upper most, black contribution), organic (middle), and sulfate (bottom).

A variety of hydrocarbons measured using a combination of TILDAS and PTR-MS are presented in Figure 3. Also in that figure, for comparison, are measurements of the total unburned hydrocarbons measured using a flame ionization detector (FID). The general agreement between the sum of the individual species and the FID is reasonably good on a ppm carbon/ppm CO_2 basis. The individual hydrocarbon measurements provide the additional insight as to which important hydrocarbons are present, from a environmental hazard perspective, and also how the hydrocarbon composition in the gas phase varies with engine power. At least for the lower engine powers, where hydrocarbon emissions are most pronounced, the most numerous individual hydrocarbons all decrease in proportion to each other and to the most prevalent hydrocarbon emissions measured: formaldehyde (by concentration) and ethylene (by mass).

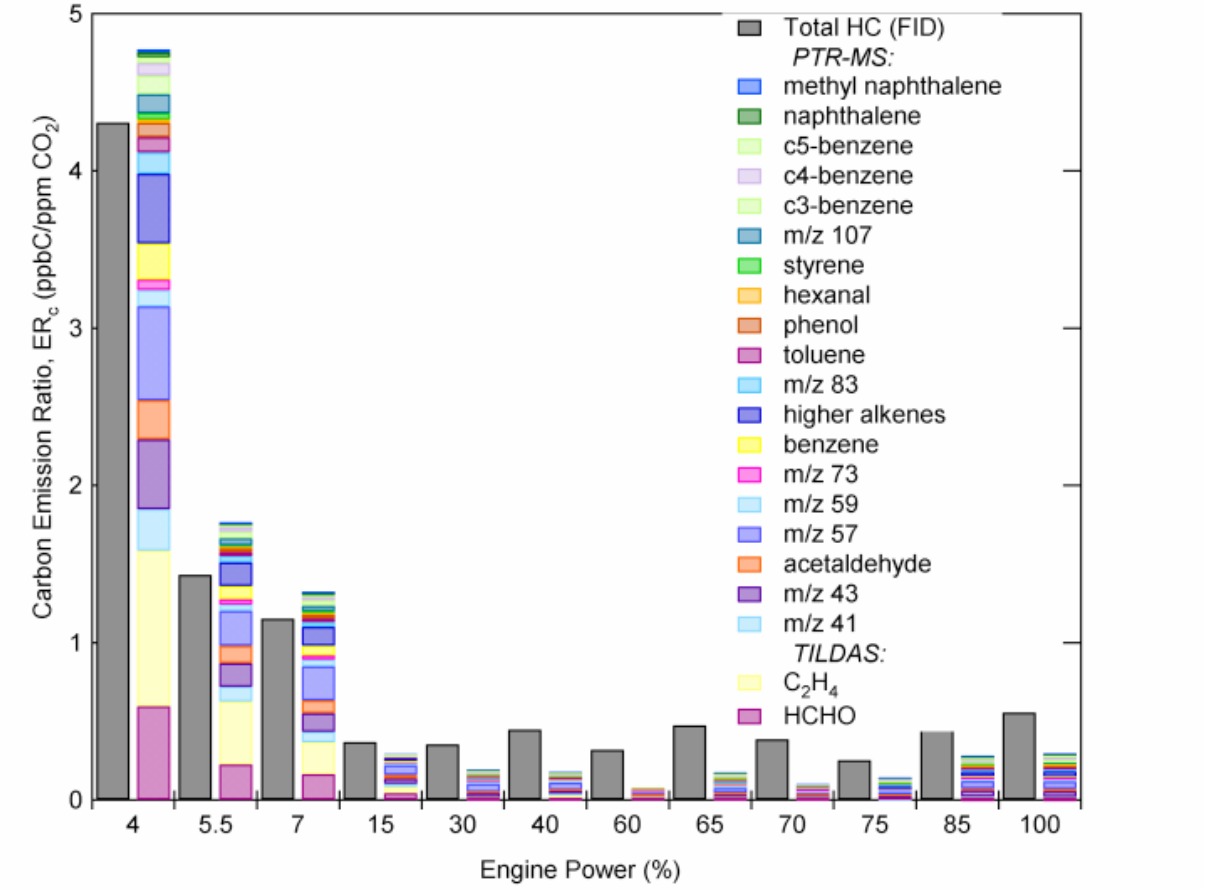

Figure 3. Hydrocarbon emissions as plotted versus engine operating power. Measurements of individual species are summed based on their carbon content (ppm C atoms) and compared to FID measurements of the total UHCs, also on a ppmC basis.

2 CONCLUDING REMARKS

Significant data has been accumulated from recent studies in characterizing aircraft emissions of particles and gases. While only a few examples of such data are presented here, the capability of measuring a wide variety of gaseous and particle parameters over a range of engine operating conditions will allow the emissions performance of aircraft engines to be quantified in great detail. This, in turn, will provide inputs to better understanding of how these emissions may impact the environment, and will permit a better evaluation of whether and to what degree any of these emissions may have important consequences for human health for populations in the proximity of airport operations.

ACKNOWLEDGMENTS

Sponsorship of NASA, CARB, FAA and the UMR Center of Excellence for Aerospace Particulate Emission Reduction Research is gratefully acknowledged. Support and interaction with the various mission team members, including airports, airlines and other research teams contributed greatly to the overall missions' successes.

REFERENCES

Anderson, B.E., H.-S. Branham, C.H. Hudgins, J.V. Plant, J.O. Ballenthin, T.M. Miller A.A. Viggiano, D.R. Blake, H. Boudries, M. Canagaratna, R.C. Miake-Lye, T.B. Onasch, J. Wormhoudt, D.R. Worsnop, K.E. Brunke, S. Culler, P. Penko, T. Sanders, H.-S. Han, P. Lee, and D.Y.H. Pui, L.K. Thornhill, and E. Winstead,, 2005: Experiment to Characterize Aircraft Volatile Aerosol and Trace-Species Emissions (EXCAVATE), NASA TM-2005-213783, NASA Langley Research Center, Hampton VA, USA, 175 pp.

ARB, 2006 The Development of Exhaust Speciation Profiles for Commercial Jet Engines, Final report in press.

Herndon, S.C., J.H. Shorter, M.S. Zahniser, D.D. Nelson, J.T. Jayne, R.C. Brown, R.C. Miake-Lye, I.A Waitz, P. Silva, T. Lanni, K.L. Demerjian, and C.E. Kolb, 2004: NO and NO_2 emission ratios measured from in-use commercial aircraft during taxi and takeoff, *Environ. Sci. Technol*. 38, 6078-6084.

Herndon, S.C., T.B. Onasch, B.P. Frank, L.C. Marr, J.T. Jayne, M.R. Canagaratna, J. Grygas, T. Lanni, B.E. Anderson, D.R. Worsnop, and R.C. Miake-Lye, 2005: Particulate emissions from in-use commercial aircraft, *Aerosol. Sci. Technol*. 39, 799-809.

Herndon, S.C., T. Rogers, E.J. Dunlea, J.T. Jayne, R.C. Miake-Lye, and B. Knighton, 2006: Hydrocarbon emissions from in-use commercial aircraft during airport operation, *Environ. Sci. Technol*. 40, 4406-4413.

Wey, C.C., B.E. Anderson, C. Hudgins, C. Wey, X. Li-Jones, E. Winstead, L.K. Thornhill, P. Lobo, D. Hagen, P. Whitefield, P. E. Yelvington, S.C. Herndon, T.B. Onasch, R.C. Miake-Lye, J. Wormhoudt, W.B. Knighton, R. Howard, D. Bryant, E. Corporan, C. Moses, D. Holve, and W. Dodds, 2006: Aircraft Particle Emissions eXperiment (APEX), NASA TM-2006-214382 and ARL-TR-3903, NASA Glenn Research Center, Cleveland OH, USA, 514 pp.

Whitefield, P.D., D. Hagen, J. Wormhoudt, R.C. Miake-Lye, C. Wilson, K. Brundish, I.A. Waitz, S. Lukachko, and C.K. Yam, 2002: NASA/QinetiQ Collaborative Program – Final Report, NASA TM-2002-211900 and ARL-CR-0508, NASA, Washington, DC, USA, 193 pp.

New Aviation Scenarios for 2050

B. Owen*, D. S. Lee, L. Lim
Dalton Research Institute, Department of Environmental and Geographical Sciences, Manchester Metropolitan University, United Kingdom

Keywords: aviation, emission scenarios, simple climate model

ABSTRACT: New emission scenarios for aviation are provided to 2050. The emission scenarios have been developed using the SRES growth assumptions and provide an update to the emission scenarios in the IPCC Special Report *Aviation and the Global Atmosphere*. The emission scenarios are input to a simple climate model to provide radiative forcing and temperature response estimates.

1 INTRODUCTION

This study has used a global model of aircraft movements and emissions (FAST) to calculate new future emissions for the time period 2000 to 2050. The SRES GDP projections are used in this study (IPCC, 2000) and the results represent an update on aviation emissions scenarios of CO_2 to 2050 made in a consistent manner with those from the IPCC's Special Report *Aviation and the Global Atmosphere,* (IPCC, 1999) which uses the older IPCC IS92 GDP projections. The FAST model (Lee *et al.,* 2005) has been used as the principal tool in this study. FAST has been used to calculate a global total of fuel, CO_2 and NO_x emissions for aviation emissions for the baseline and future scenarios to 2050. The results are global spatially resolved, 3 D global emissions inventories (1^o by 1^o grid with 610 m vertical resolution). The aviation emissions for the SRES A1 and B1 marker scenarios have been used as input to a linear climate response model LinClim (Lim *et al*, 2006) to produce the associated radiative forcing and temperature response values.

2 THE FAST MODEL

The FAST model works by combining a global aircraft movements database with data on fuel flow provided by a separate commercial model PIANO, which is an aircraft performance model (Simos, 2004). These data with knowledge on aircraft and engine types, allow calculation of emissions via a recognized and validated algorithm that corrects ICAO LTO Certification Data for altitude. Baseline calculations have used the year 2000 and these calculations have been undertaken using the OAG global aircraft movement database. Future fleet predictions are made using the FAST model. The model requires the characteristics of hypothetical future generic aircraft to be defined. The FAST methodology imposes the restriction that any hypothetical aircraft must be based on a configuration that can be generated using the PIANO aircraft performance program. Whilst this approach ensures that the resulting aircraft characteristics remain within the realm of reality, for a future scenario one might wish to project these characteristics beyond the limits set by PIANO. For this reason, a scaling factor can be applied to fuel consumption. This factor is applied uniformly (*i.e.* to all phases of the flight cycle).

Future aircraft movements have been calculated using the ICAO (CAEP) forecasts (Wickrama *et al,* 2003) in conjunction with the IPCC SRES GDP growth assumptions. The ICAO traffic forecasts to 2020 of revenue passenger kilometers (RPK) and seat kilometres offered (SKO) have been used directly. The ICAO SKO forecasts are provided regionally and according to the seat-banding of the aircraft. The forecast totals are summarized in Table 1.

* *Corresponding author:* Bethan Owen, Dalton Research Institute, Department of Environmental and Geographical Sciences, Manchester Metropolitan University, Manchester M1 5GD, United Kingdom. Email: b.owen@mmu.ac.uk

Table 1. ICAO Long Term Global Forecasts (FESG/CAEP6, 2003)

	2005	2010	2015	2020
Seat kilometers offered (SKO) in billions	4685	5998	7542	9365
Revenue passenger kilometers (RPK) in billions	3304	4312	5508	7050

In order to provide future fleet predictions, the carrying capacity of freight also needs to be considered. The ICAO forecast in Table 1 does not include freight and relates to passenger traffic only. The OAG movements data used for the base case do include freight movements but they are not identified explicitly. A simple methodology was devised to include freight. A comparison of time series of RPK from 1970 to 1995 used by the IPCC (1999) was compared with the ICAO RPK (passenger movements only) for the same period. A linear relationship was apparent between the two data sets and a factor of 1.16 was derived that was taken to represent the freighter movements (in terms of RPK) in the IPCC data. This factor when applied to the ICAO 2000 data also brought the ICAO RPK up to the OAG 2000 RPK value (used as the base case in this study). The factor was applied to all scenarios and years which is clearly a simplistic approach bearing in mind that the passenger and freight growth can be very different.

For dates after 2020, an alternative approach is used, similar to the IPCC (1999) methodology, whereby a global relationship between RPK and GDP is used according to a non-linear regression model and predicting SKO from SRES A1 and B2 GDP data. A logistics growth curve was derived using published ICAO traffic statistics and UN GDP statistics from 1970 to 2000.

The model was used to extrapolate future global RPK values from 2020 to 2050 using the SRES GDP global growth scenarios A1 and B2. The SRES scenarios A1 and B2 were chosen as the main ones for calculation of emissions as IPCC is currently using these as "baselines" against which mitigation possibilities are being considered by its Working Group 3. Selection of other SRES scenarios would give different results. A wider range is explored in terms of RPK projections (including A2 and B1) but the step from RPK to emissions involves much computation and hence the two main scenarios focused upon A1 and B2 in terms of their GDP projections.

Table 2. Annual average percentage growth factors for global GDP growth forecasts (IPCC, 2000)

Scenario	2020–2030	2030–2040	2040–2050
SRES A1B-AIM	4.66	3.52	3.71
SRES A2	2.36	3.52	1.21
SRES B1	3.35	3.26	3.02
SRES B2	2.67	2.62	2.50
IS92a	2.3	2.3	2.3
IS92c	1.2	1.2	1.2
IS92e	3.0	3.0	3.0

The SRES GDP data are provided at 10 yearly intervals as shown in Table 2 and these data were applied for the 2020-2050 period to provide global projections of RPK (Table 3). The SRES A1B scenario produces the highest GDP growth over this period, higher than the IS92e (high growth scenario) leading to higher predictions of RPK. The A2 and B2 scenarios produce similar RPK projections to the IS92Fa (medium growth) scenario in 2050. None of the selected SRES scenarios resulted in projections as low as the IS92Fc (low growth) scenario.

Table 3. RPK projections for SRES and IS92 a, c and e GDP growth forecasts (in billions)

Year	A1B	A2	B1	B2	IS92a	IS92e	IS92c
2020	7042	7042	7042	7042	6553	8302	5071
2050	24407	16896	21632	18100	13934	21978	7817

Table 4. Traffic efficiency (as SKO/kg of fuel) improvement in percent per year

Time Period	Improvement (percent per year)
2000-2010	1.3
2010-2020	1.0
2020-2050	0.5

Future trends in traffic efficiency improvements from the IPCC report (IPCC, 1999) are shown in Table 4. These "efficiencies" include improvements arising from the introduction of new aircraft into the fleet and changes to operating conditions and passenger management i.e. not simply a change in engines but the overall operational efficiency of the engine/airframe/passenger management. The FAST model requires a fuel factor input that can be changes to account for future improvements in the fuel efficiency of the aircraft. This is different to the overall traffic efficiency described above, as this relates only to the technological improvements and not changes in fleet or passenger management. For the purposes of this study it was necessary to prescribe a fuel factor based on technological improvements independent of the operation of the fleet. The factors shown in Table 5 below together with the forecast changes in aircraft size etc from the CAEP forecasts produce the improvements in traffic efficiency commensurate with those improvements given in Table 4.

Table 5. Fuel factor assumptions applied to future periods

Period	Fuel factor
2005	1
2020	0.84
2030	0.80
2040	0.76
2050	0.72

3 EMISSION SCENARIO RESULTS

The results of the FAST emission scenarios are shown in Figure 1. The FAST-A1 2050 results lie just above the IPCC (1998) Fe1 (high) scenario, whilst FAST-B2 is greater than the mid-range Fa1 scenario. For 2040 and 2050 the updated SRES A1B traffic projections and hence emissions are larger than those derived from the IS92 GDP assumptions. The SRES GDP growth rates are similar to the IS92 values however, application of the ten year average growth rates generally exceed the equivalent but longer term IS92 growth rates producing higher traffic and ultimately higher emission estimates. The FAST-A1 emission estimates are in the order of five times greater than the 2000 emissions and the FAST-B2 estimates are approximately 3 times greater than the 2000 emissions. The CONSAVE (2005) scenarios 'ULS' (Unlimited Skies) is consistent with SRES A1 and has slightly higher values than the FAST-A1 estimates.

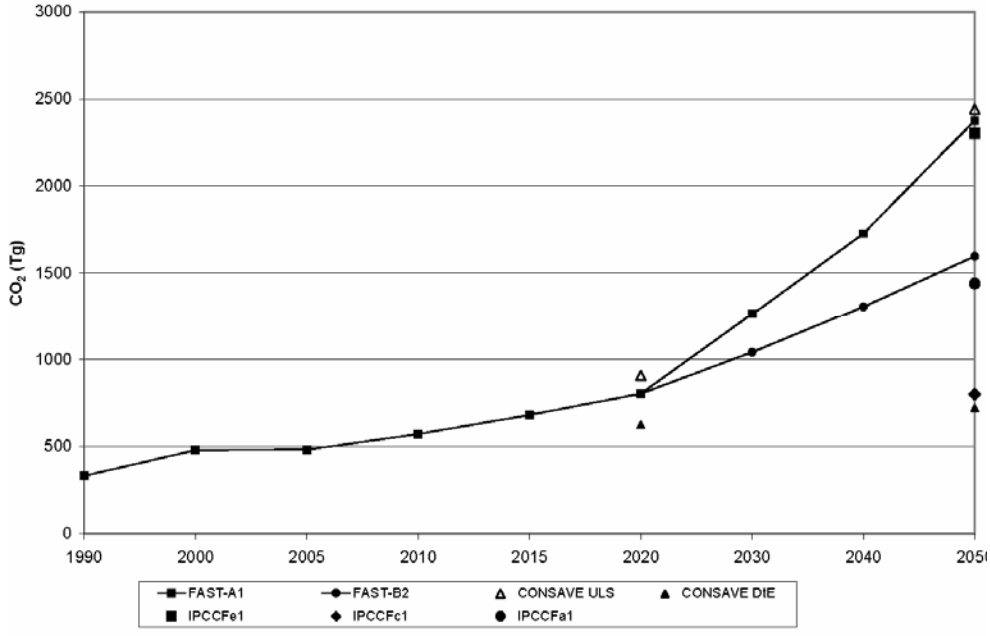

Figure 1. Comparison of global aviation CO_2 emissions (Tg yr^{-1}), 1990 to 2050 using FAST and showing other estimates for 2020 and 2050.

4 THE LINCLIM MODEL

The resultant emission scenarios were scaled by appropriate scaling factors to account for systematic underestimation of fuel due to great circle routing, military aviation and non-scheduled traffic, as in the IPCC (1999) work. The emissions have then been applied to the LinClim model which is a linear climate response model formulated to calculate radiative forcing (RF) and temperature response (Lim et al., 2006). Aviation emissions post-2050 are assumed to grow at a rate of 1% per annum to 2100 (Sausen and Schumann, 2000). Background CO_2 concentrations corresponding to each SRES scenario have been used for CO_2 RF and temperature response calculations and the RF for other perturbations were scaled to reference year 2000 values published by Sausen et al., 2005. The temperature response uses climate sensitivity parameter of 0.64 K/Wm^{-2} and the efficacies published by Ponater et al., 2006: i.e. CO_2, SO_4, and BC 1; O_3 1.37; CH_4 1.18; H_2O 1.14 and contrails 0.59.

5 RESULTS

The estimated RF values associated with the emission scenarios are shown in Figure 2 together with the RF values associated with the IPCC (1999) Fa1, Fc1 and Fe1 emission scenarios (Sausen and Schumann, 2000). The temperature response values associated with the emission scenarios are shown in Figure 3.

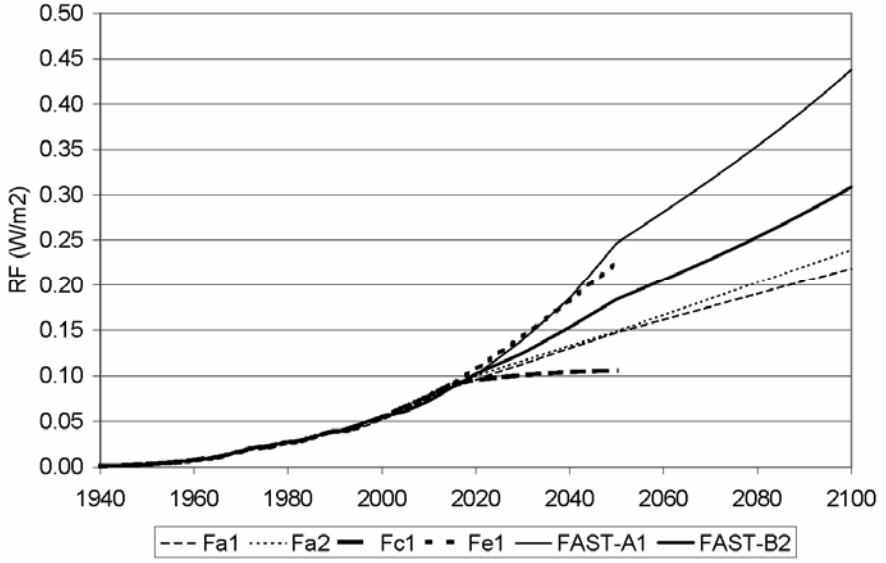

Figure 2. RF values for emission scenarios produced using LinClim.

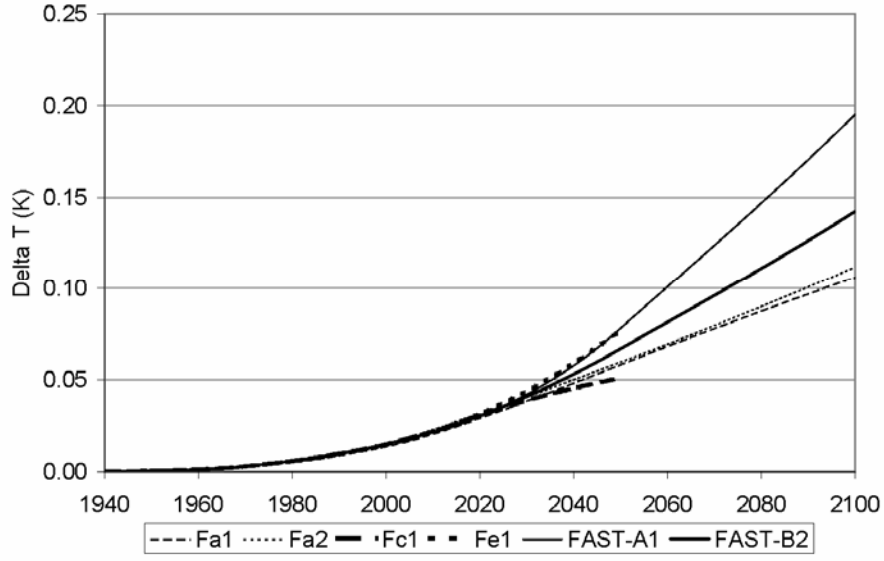

Figure 3. Temperature response values for emission scenarios produced using LinClim.

6 CONCLUSIONS AND FUTURE WORK

The 2050 FAST-A1 and FAST-B2 scenarios provided here show an initial update of the FESG work incorporating the SRES GDP growth assumptions. The CO_2 RF values associated with the A1 SRES marker and IPCC Fe1 emission scenarios in 2050 are 0.247 Wm^{-2} and 0.225 Wm^{-2} respectively. The corresponding temperature response in 2050 is calculated as 0.0795 K for the FAST-A1 emission scenario and 0.0772 K for the IPCC Fe1 scenario. In 2100, the temperature response values associated with the FAST–A1 and FAST-B2 aviation scenarios are calculated to be 0.1953 K and 0.1425 K respectively.

The next step in this work will be to review the technology assumptions with regard to fuel use and NO_x emission indices in the light of the most recent research and the industry technology targets. Further development of the traffic growth at a regional level consistent with the SRES A1 and B2 storylines is also underway.

REFERENCES

CONSAVE (2005) Final Technical Report Berghof R., A. Schmitt C. Eyers, K. Haag, J. Middel, M. Hepting, A. Grübler, R. Hancox G4MA-CT-2002-04013 July 2005

IPCC (1999) Aircraft emissions: current inventories and future scenarios. Chapter 9 of *Aviation and the Global Atmosphere* J.E. Penner, D.H. Lister, D.J. Griggs, D.J. Dokken and M. McFarland (Eds) Special Report of the Intergovernmental Panel on Climate Change, Cambridge University Press, Cambridge.

IPCC (2000) Emission Scenarios: A Special Report of Working Group3 of the Intergovernmental Panel on Climate Change, Cambridge University Press, Cambridge.

Lee, D.S., B. Owen, C. Fichter, L. Lim and D. Dimitriu (2005): Allocation of International aviation emissions from scheduled air traffic – present day and historical (report 2 of 3). Manchester Metropolitan University, Centre for Air Transport and the Environment, CATE-2005-3[c]-2, Manchester, UK.

Lim, L.L., D.S. Lee, R. Sausen and M. Ponater, 2007: Quantifying the effects of aviation on radiative forcing and temperature with a climate response model. This volume.

Ponater, M., S. Pechtl, R. Sausen, U. Schumann and G. Hüttig, 2006: Potential of the cryoplane technology to reduce aircraft climate impact: A state-of-the-art assessment. *Atmos. Environ 40*, 6928–6944.

Sausen, R. and U. Schumann, 2000: Estimates of the climate response to aircraft CO_2 and NO_X emissions scenarios. *Clim. Change 44*, 27–58.

Sausen, R., I. Isaksen, V. Grewe, D. Hauglustaine, D.S. Lee, G. Myhre, M.O. Köhler, G. Pitari, U. Schumann, F. Stordal and C. Zerefos, 2005: Aviation radiative forcing in 2000: and update on IPCC (1999). *Meteorol. Zeit. 114*, 555–561.

Simos D., 2004: PIANO: PIANO users guide version 4.0, Lissys Limited, UK (www.piano.aero).

SPIDER model process studies of aircraft plume dilution using simplified chemistry

N. Dotzek*, R. Sausen
DLR-Institut für Physik der Atmosphäre Oberpfaffenhofen, Germany

Keywords: Aircraft emissions, plume dilution, simplified chemistry, effective emission indices.

ABSTRACT: The box model SPIDER was developed to test and compare various approaches to include the effect of aircraft plume processes (effective emissions indices) in large scale chemistry transport models and climate-chemistry models. Its simplified NO_x-O_3 chemistry parameterises only the most relevant non-linear processes. SPIDER reproduces the main features of more sophisticated plume models. Multi-plume interactions illustrate the capability of the SPIDER model.

1 MOTIVATION

Emissions from aircraft impact on global climate (cf. Brasseur et al., 1998; IPCC, 1999; Sausen et al., 2005). They are usually implemented in General Circulation Models (CGM) or Chemistry Transport Models (CTM) by an instantaneous dispersion of the emitted matter over the large-scale grid boxes. Following Petry et al. (1998), this is called the instantaneous dispersion (ID) approach. The ID approach neglects non-linear chemical conversion processes in the evolving single plume. To resolve these by a plume model is called the single plume, or SP approach. However, detailed SP chemical modelling is computationally too demanding, both for more complex principle studies of plume-plume interaction in a grid box, and for operational implementation in large-scale models.

For improvement of the ID approach in GCMs, Effective Emission Indices (EEIs) can be used (e.g., Möllhoff, 1996; Petry et al., 1998). These, and several other approaches to the problem, e.g., by Meijer et al. (1997), Karol et al. (1997, 2000), Kraabøl et al. (2000) and Kraabøl and Stordal (2000) all applied detailed chemistry schemes, while a simplified model to test and compare the various EEI concepts, and to perform studies of multi-plume interactions remains desirable.

The present paper reports on the development of such a box model with simplified chemistry, the SPIDER (SP-ID Emission Relations) model. The following sections focus on setup of the model, validation and first application to a plume-plume interaction. Further model development and applications will be described in a forthcoming paper.

Motivated by the work by Petry et al. (1998) who applied a detailed chemistry scheme, we aim at computing plume dilution, and comparing of ID and SP results using a computationally efficient box model with greatly simplified chemistry. The resulting SPIDER model avoids explicit solution of the chemical rate equations. Chemistry enters the equations only in parameterized form by "dynamic forcing" terms, and the only species considered are NO_x and O_3.

The objectives are to apply the validated SPIDER model to more complex cases, e.g. multiple plumes or the interaction between neighbouring GCM grid cell NO_x or O_3 fields, and to eventually evaluate different EEI approaches.

1.1 *SPIDER model setup*

The main process to be covered by the model is the non-linear production of ozone by aircraft NO_x emissions at cruise altitude. Hence, the first simplification in the SPIDER system of equations is to include only these two species: NO_x and O_3.

The physical processes which are to be explicitly included in and resolved by the model within a typical GCM grid box volume are a) the emission of NO_x inside the GCM box, S_{NOx}, b) non-linear production of ozone, P_{O3}, and c) the decay of the NO_x and O_3 fields by conversion to reservoir spe-

* *Corresponding author:* Nikolai Dotzek, DLR-Institut für Physik der Atmosphäre, Oberpfaffenhofen, D-82234 Wessling, Germany. Email: nikolai.dotzek@dlr.de

cies. For treatment of the SP approach, additionally the background (outer domain, superscript o) and plume fields (inner domain, superscript i) have to be integrated separately, and the entrainment of background matter by turbulent mixing at the growing-plume boundary enters as another individual term in the budget equations.

1.1.1 *ID budget equations*

In Eqs. (1-4), the following units hold $[NO_x]$ = mol, $[O_3]$ = mol, $[no_x]$ = nmol mol^{-1}, following the well-known convention to denote extensive quantities by upper-case, and intensive quantities by lower-case letters:

$$d_t\, NO_x = S_{NOx}\, \delta(t-t') - \frac{1}{\tau_{NOx}} NO_x \quad , \tag{1}$$

$$d_t\, O_3 = P_{O3}(no_x) \qquad - \frac{1}{\tau_{O3}} O_3 \quad . \tag{2}$$

The reference background state without aircraft emissions follows for $S \equiv 0$, and d_t denotes the temporal derivative *d/dt*.

The decay, or conversion of NO_x and O_3 to reservoir species, is modeled as an exponential decay with fixed half-time periods τ (τ_{NOx} = 10 days, τ_{O3} = 30 days, cf. Köhler and Sausen, 1994). Future versions of SPIDER will include a typical diurnal variation of these time scales, but this is a second-order effect, and neglecting the diurnal cycle here has little consequence on the results.

1.1.2 *SP budget equations*

In Eqs. (3) and (4), each species must be treated with one budget equation for the plume (superscript i) and the background (superscript o). As the box model reference volume is one GCM grid box, the computation of entrainment, with a linear plume growth rate, in Eqs. (3-4) is terminated as soon as the plume volume V^i is equal to the reference volume V_{GCM}.

$$d_t\, NO_x{}^i = S_{NOx}\, \delta(t-t') + NO_x{}^o / V^o\, d_t V^i - \frac{1}{\tau_{NOx}} NO_x{}^i \quad , \tag{3a}$$

$$d_t\, NO_x{}^o = \qquad - NO_x{}^o / V^o\, d_t V^i - \frac{1}{\tau_{NOx}} NO_x{}^o \quad , \tag{3b}$$

$$d_t\, O_3{}^i = P_{O3}(no_x{}^i) \qquad + \; O_3{}^o / V^o\, d_t V^i - \frac{1}{\tau_{O3}} O_3{}^i \quad , \tag{4a}$$

$$d_t\, O_3{}^o = P_{O3}(no_x{}^o) \qquad - \; O_3{}^o / V^o\, d_t V^i - \frac{1}{\tau_{O3}} O_3{}^o \quad . \tag{4b}$$

Eq. (3a) allows including the case in which a fresh aircraft plume is emitted along the axis of an aged plume emitted by another aircraft earlier on. This case was already investigated by Kraabøl and Stordal (2000), and will also be treated here in Sec. 3.2

1.2 *Parameterisation of $P_{O3}(no_x)$ terms*

The non-linear production of ozone as a function of the ambient NO_x concentrations remains to be specified for the SPIDER model equations (2) and (4). As treated in detail by, e.g., Johnson and Rohrer (1995), Brasseur et al. (1996), Grooß et al. (1998), and Meilinger et al. (2001), the production of ozone does not only depend on NO_x concentrations, but is a highly variable function of other species like O_3 itself, H_2O, CO, hydrocarbons, state variables *p*, and *T*, and the actinic flux *J*. A perfect parameterisation in this multidimensional phase space is impossible, and likely has prevented earlier studies using simplified chemistry studies of aircraft plume dilution.

However, in the present context, the objective is to develop a model which allows for principle studies of plume dilution, plume interaction, and methods to derive EEIs. Hence, a parameterisation of ozone production as a function of nitrogen oxides for some typical atmospheric conditions at cruise altitude following the data presented in the literature is possible. Aside from the NO_x concen-

tration, also the solar elevation angle must be taken into account, in order to capture the diurnal cycle of photochemical ozone production.

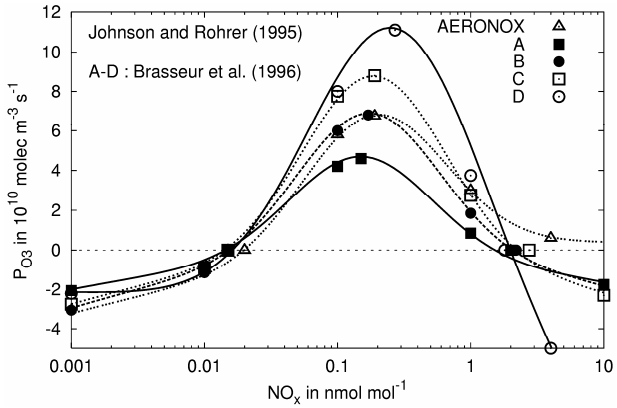

Figure 1. Net ozone production rate P_{O3} as a function of ambient NO_x concentration. The symbols are data from Johnson and Rohrer (1995) from the AERONOX project, and from Brasseur et al. (1996). The curves are fits to these data and form the selectable SPIDER P_{O3} parameterisations.

Figure 1 shows five different parameterisations of which D was selected in the SPIDER model. Curve D from the Brasseur et al. (1996) data includes effects of the diurnal cycle, the other curves are very similar in shape, and their variation comes mainly from different ambient chemical conditions.

Note the non-linearity, or rather non-monotonicity, of all P_{O3} curves. Low and very high NO_x concentrations are characterized by ozone depletion, while the peak ozone production is found in the range of 0.15 to 0.27 nmol mol^{-1}. The fact that the shape of the curves is quite uniform in the upper troposphere gives us some confidence that the SPIDER parameterisation of P_{O3} holds in a general sense and is adequate for principle process studies.

2 RESULTS

Here, we present the SPIDER model validation and its first application of multiple plume effects.

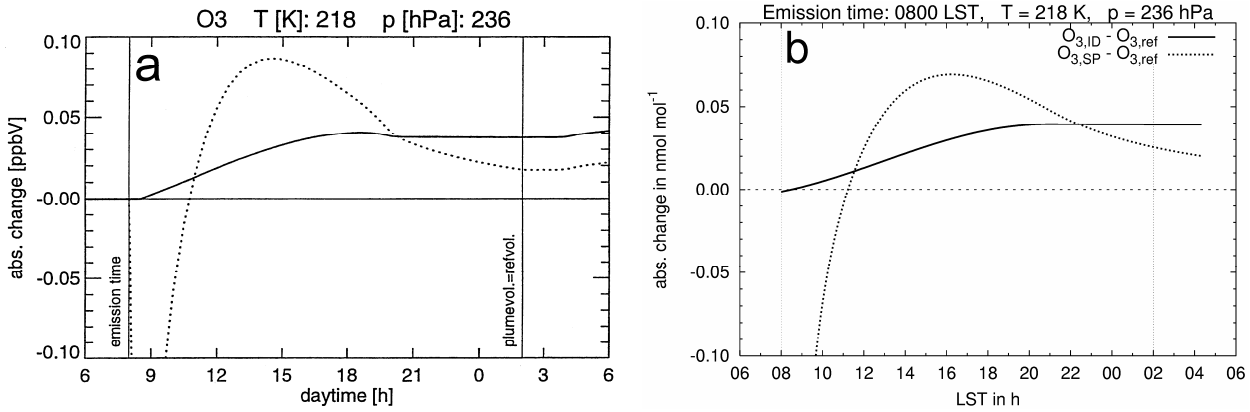

Figure 2. Absolute aircraft-induced change of O_3 concentration compared to the background state for ID (solid) and SP simulations (dotted). (a) is from Möllhoff (1996), (b) shows the corresponding SPIDER run.

2.1 *SPIDER model validation and sensitivity*

We used the original model cases from the work by Möllhoff (1996) to validate the SPIDER model. There, without wind shear or cross-plume wind components, the exhaust of a typical B747 airplane was emitted as a line-source at 0800 LST (local solar time) in a V_{GCM} = 50 x 50 x 1 km^3 reference volume. Ambient conditions were mid-latitude summer, T = 218 K and p = 236 hPa (about 10 km above see level, ASL). The initial values of NO_x and O_3 in the plume were chosen to be representative of the early dispersion regime (about 100 s after emission). Linear plume growth was specified such that after 18 h of plume dilution, the plume volume was equal to the reference volume V_{GCM}.

Figure 2b shows that the qualitative behaviour of the Möllhoff (1996) simulation in Figure 2a is captured well by the SPIDER model. The quantitative agreement is adequate; the main difference is that in the SP simulation, the peak change in O_3 is at a lower level and slightly later for the SPIDER run. For the ID run, the small peak before converging to the night time stable state is not resolved by SPIDER; instead, it merely converges towards the night time conditions.

The first few minutes after plume emission are characterised by ozone titration within the plume due to the very high NO_x concentrations (cf. Fig. 1, curve D). As the SPIDER model equations are formulated for the plume dispersion regime (the far-field solution), they cannot resolve the initial titration, which is a near-field plume process. Following Veenstra and Beck (1994), the initial ozone level in the plume must be lowered slightly compared to the background state to provide the proper initialisation values for the early dispersion regime[1].

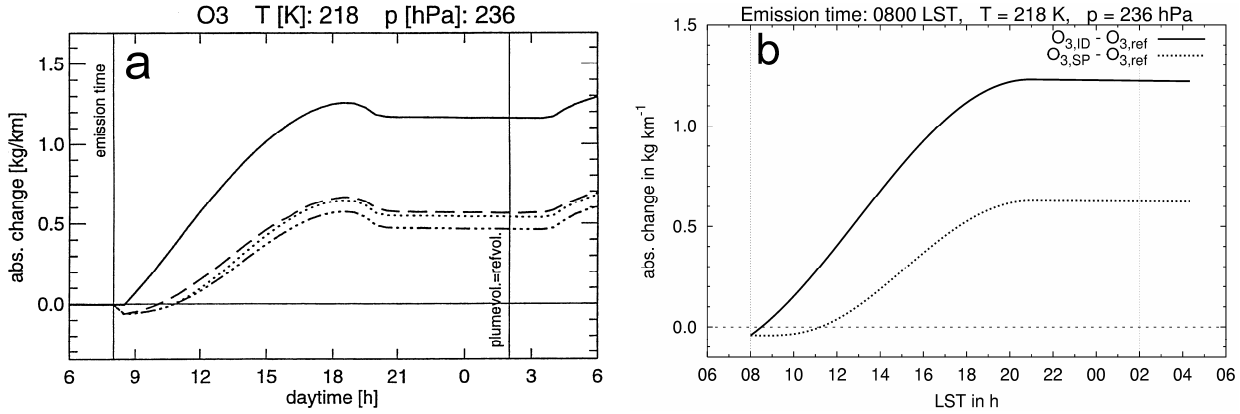

Figure 3. As Figure 2, but for the absolute change in O_3 mass per kilometre plume along the flight path. The dashed and dash-dotted lines in (a) from Möllhoff (1996) are not interpreted here.

Figure 3 shows the comparison between Möllhoff (1996) and the SPIDER results in terms of ozone mass difference per kilometre plume. Again, the small peak just before reaching the night time levels with zero photochemistry is not reproduced by SPIDER. Otherwise, the qualitative and quantitative agreement is good. Note that SPIDER correctly shows the extended period of negative change in ozone between 0800 and 1100 LST, and that the night time levels are well-captured.

2.2 *Aircraft following on track of initial one*

The first SPIDER model application case is a second, identical, aircraft exactly following the track of the first one after 4.5 h, injecting (and instantaneously distributing) a fresh plume into the aged, diluted one. For regions like the North Atlantic flight corridor, we consider this scenario to be quite realistic. Then, ID and SP simulations are continued and compared to the reference run. A similar case was investigated by Kraabøl and Stordal (2000), but for emission of the young plume 1 h after the first one (and additional runs for 2 h and 3 h release time lag).

Figure 4 shows the effects for the absolute change in ozone concentration (a) and mass per kilometre plume (b). The results should be compared to the reference case in Figs. 2b and 3b. The immediate effect of the young plume is visible in both panels by the initial drop in ozone due to titration. After recovery, the rate of ozone production is significantly enhanced, and higher night time levels of ozone result. For the ozone changes in Figure 4, the enhancement is about 50% for both the ID and SP runs, and for both the concentration and mass changes.

The response to the increase in aircraft NO_x is not linear here (in contrast to GCM simulations, cf. Grewe et al., 1999), as SPIDER experiences the full non-linearity of the P_{O3} term due to the initially high NO_x concentrations. I.e., the ozone production is not doubled by injection of the second plume after 4.5 h. Yet what can be said is that the gap between the results of the ID and SP approaches widens by roughly 50% due to the interaction of the two plumes. Thus, conclusions derived from single plume comparisons between SP and ID results, like that of Petry et al. (1998) stat-

[1] For completeness, we note that SPIDER is capable of reproducing initial ozone titration when the ozone concentration in the plume is initialised to the reference value. However, this titration is much weaker than that of Fig. 2

ing that for diurnal or seasonal averages, the difference between SP and ID plume dilution is not significant, may not remain justified in regions with frequent interaction of plumes.

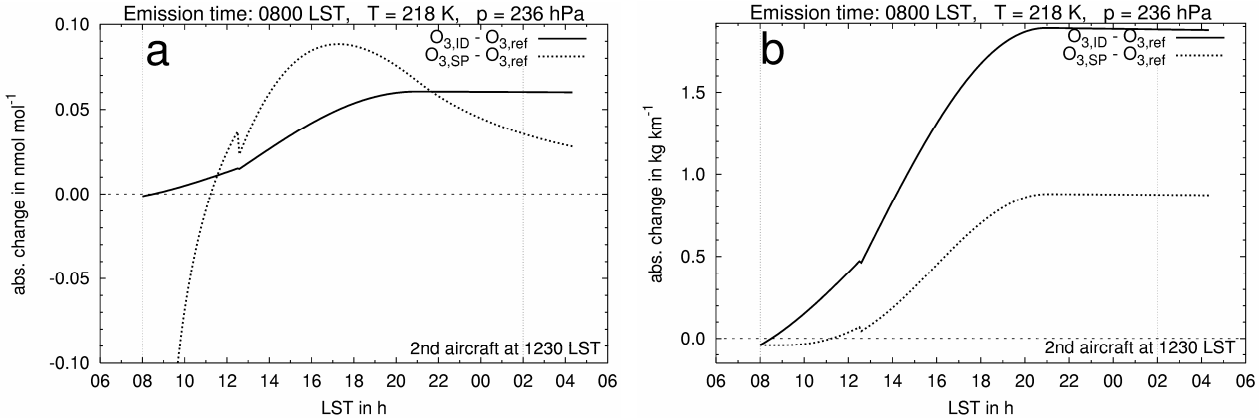

Figure 4. As Figs. 2b (a) and 3b (b), but with a second, identical aircraft plume emitted along the original flight path 4.5 h after emission of the first plume. Emission time 0800 LST is marked by the dotted line.

3 DISCUSSION

The SPIDER model could be validated in the framework of its simplifying assumptions. The basic plume dilution processes are well represented, in part even quantitatively. Some details are missing in the model which would require the complete set of chemical reactions – or an improved description of either the plume growth (being linear only on average, cf. Schumann et al., 1998) or the actinic flux in the P_{O3} term. These latter points are current work in SPIDER development.

In our simulation of interaction of two coaxial plumes, a net increase in produced ozone was found, and the gap between SP and ID approaches widened. Kraabøl and Stordal (2000) did a similar study, but for emission of the young plume 1 h after the old one. They employed a full chemistry model, slightly different release time (0700 LST), and other initial values of plume and background NO_x and O_3 concentrations. In contrast to our findings, they reported a net decrease in ozone compared to the single-plume run, and less conversion of the emitted NO_x. Qualitatively similar results were reported for secondary plume release after time lags of 2 h and 3 h, respectively.

There may be several reasons for these differences to our SPIDER results. Kraabøl and Stordal (2000) emitted their second model plume in ambient conditions characterised by very high NO_x concentrations (6.8 nmol mol^{-1}). Without further debate on the realism of these high NO_x values for 1 to 3 h old plumes, their young plume experienced conditions of strong ozone titration (cf. Fig. 1). In the SPIDER model run 4.5 h after emission of the first plume, the aged plume NO_x concentration is well below 2 nmol mol^{-1}, i.e., definitely in a region of the P_{O3} term of Figure 1 with at least weak ozone production. Besides, Kraabøl and Stordal (2000) compared their plume concentrations with background conditions which changed with time on injection of the second plume. In the present SPIDER case, the background was not altered after introduction of the young plume, in order to be able to compare the results to the single-plume reference run.

4 CONCLUSIONS

Our study using the SPIDER box model showed:

- The model is well-suited for principle studies, and could be validated qualitatively and in part quantitatively using results by Möllhoff (1996) and Petry et al. (1998);
- The model reproduces the high sensitivity to plume and background NO_x and O_3 concentrations;
- Multi-plume interactions can alter the gap between of ID and SP plume dilution approaches.

Aside from more complex multi-plume and GCM grid box interactions, future work will encompass refinement of the computation of plume growth, actinic flux, and NO_x or O_3 decay times.

ACKNOWLEDGMENTS

We are grateful to Johannes Hendricks for further information on the Möllhoff (1996) simulations and for commenting on a draft of this paper. This work was partly funded by the European Commission in the FP6 integrated project QUANTIFY under contract no. 003893 (GOCE).

REFERENCES

Brasseur, G. P., J.-F. Müller, and C. Granier, 1996: Atmospheric impact of NO_x emissions by subsonic aircraft: A three-dimensional model study. *J. Geophys. Res*., 101 D, 1423-1428.

Brasseur, G. P., R. A. Cox, D. Hauglustaine, I. Isaksen, J. Lelieveld, D. H. Lister, R. Sausen, U. Schumann, A. Wahner, and P. Wiesen, 1998: European scientific assessment of the atmospheric effects of aircraft emissions. *Atmos. Environ*., 32(13), 2329-2418.

Grewe**,** V., M. Dameris, R. Hein, I. Köhler, and R. Sausen, 1999: Impact of future subsonic aircraft NO_x emissions on the atmospheric composition. *Geophys. Res. Lett. 26***,** 47–50.

Grooß, J.-U., C. Brühl, and T. Peter, 1998: Impact of aircraft emissions on tropospheric and stratospheric ozone. Part I: Chemistry and 2-D model results. *Atmos. Environ*., 32(18), 3173-3184.

IPCC, 1999: Aviation and the global atmosphere. – A special report of IPCC working groups I and III. (Penner, J. E., D. H. Lister, D. J. Griggs, D. J. Dokken, and M. McFarland (eds.)). Intergovernmental Panel on Climate Change. – Cambridge University Press, Cambridge, UK and New York, NY, USA, 365 pp.

Johnson, C., and F. Rohrer, 1995: NO_x and O_3 chemistry in the upper troposphere and lower stratosphere. In: Schumann (1995), 325-335.

Karol, I. L., Y. E. Ozolin, and E. V. Rozanov, 1997: Box and Gaussian plume models of the exhaust composition evolution of subsonic transport aircraft in- and out of the flight corridor. *Ann. Geophys. 15*, 88-96.

Karol, I. L., Y. E. Ozolin, A. A. Kiselev, and E. V. Rozanov, 2000: Plume transformation index (PTI) of the subsonic aircraft exhausts and their dependence on the external conditions. *Geophys. Res. Lett. 27(3)*, 373-376.

Kraabøl, A. G., and F. Stordal, 2000: Modelling chemistry in aircraft plumes 2: The chemical conversion of NO_x to reservoir species under different conditions. *Atmos. Environ. 34*, 3951-3962.

Kraabøl, A. G., P. Konopka, F. Stordal, and H. Schlager, 2000: Modelling chemistry in aircraft plumes 1: Comparison with observations and evaluation of a layered approach. *Atmos. Environ. 34*, 3939-3950.

Köhler, I., and R. Sausen, 1994: On the global transport of nitrogen oxides from emissions of aircraft. In: Schumann and Wurzel (1994), 193-198.

Meijer, E. W., P. F. J. van Velthoven, W. M. F. Wauben, J. P. Beck, and G. J. M. Velders, 1997: The effects of the conversion of nitrogen oxides in aircraft exhaust plumes in global models. *Geophys. Res. Lett*. 24(23), 3013-3016.

Meilinger, S. K., B. Kärcher, R. von Kuhlmann, and T. Peter, 2001: On the impact of heterogeneous chemistry on ozone in the tropopause region. *Geophys. Res. Lett*. 28(3), 515-518.

Möllhoff, M., 1996: Modellierung der chemischen Umwandlung reaktiver Flugzeugabgase im Tropopausenbereich unter Berücksichtigung ihrer Dispersion. Diploma thesis, Institut für Geophysik und Meteorologie, Universität zu Köln, 110 pp.

Petry, H., J. Hendricks, M. Möllhoff, E. Lippert, A. Meier, A. Ebel, and R. Sausen, 1998: Chemical conversion of subsonic aircraft emissions in the dispersing plume: Calculation of effective emission indices. *J. Geophys. Res*. 103 (D5), 5759-5772.

Sausen, R., Isaksen, I., Grewe, V., Hauglustaine, D., Lee, D.S., Myhre, G., Köhler, M.O., Pitari, G., Schumann, U., Stordal, F., Zerefos, C., 2005: Aviation radiative forcing in 2000. An update on IPCC (1999). *Meteorol. Z. 14*, 555–561.

Schumann, U. (Ed.), 1995: The impact of NO_x emissions from aircraft upon the atmosphere at flight altitudes 8 - 15 km (AERONOX). Final report to the Commission of the European Communities, 471 pp.

Schumann, U., and D. Wurzel (Eds.), 1994: Impact of emissions from aircraft and spacecraft upon the atmosphere. DLR Mitteilung 94-06, DLR, Köln, 496 pp.

Schumann, U., H. Schlager, F. Arnold, R. Baumann, P. Haschberger, and O. Klemm, 1998: Dilution of aircraft exhaust plumes at cruise altitudes. *Atmos. Environ. 32*, 3097-3103.

Veenstra, D., and J. Beck, 1994: An aircraft exhaust plume model. In: Schumann and Wurzel (1994), 286-291.